International Journal of Hydrogen Energy 72 (2024) 820–831

Contents lists available at ScienceDirect

International Journal of Hydrogen Energy

journal homepage: www.elsevier.com/locate/he

Pt-decorated tantalum oxide on mesoporous carbon supports for enhanced mass activity and start-stop and load cycling durability in PEFCs

R. Nishiizumi [a], T. Ogawa [a], K. Sanami [a], M. Yasutake [a,b], Z. Noda [c], S.M. Lyth [b,d], M. Nishihara [b,c], J. Matsuda [b,c], K. Sasaki [a,b,c,*]

[a] Department of Hydrogen Energy Systems, Faculty of Engineering, Kyushu University, Motooka 744, Nishi-ku, Fukuoka, 819-0395, Japan
[b] Next-Generation Fuel Cell Research Center (NEXT-FC), Kyushu University, Motooka 744, Nishi-ku, Fukuoka, 819-0395, Japan
[c] International Research Center for Hydrogen Energy, Kyushu University, Motooka 744, Nishi-ku, Fukuoka, 819-0395, Japan
[d] Department of Chemical and Process Engineering, University of Strathclyde, 79 Montrose Street, Glasgow, G1 1XJ, United Kingdom

ARTICLE INFO

Handling Editor: Shohji Tsushima

Keywords:
Polymer electrolyte fuel cells
Cathode catalyst
Tantalum oxide support
Mesoporous carbon
Start-stop cycle durability
Load cycle durability

ABSTRACT

Unique Pt/TaO_x/MC cathode electrocatalysts for polymer electrolyte fuel cells (PEFCs) are developed using partially-reduced TaO_x decorated on mesoporous carbon (MC). An initial mass activity (MA) of more than 500 A g^{-1} was observed for a TaO_x/MC support heat treated at 700 °C in H_2 or 1300 °C in Ar, more than double that of a conventional Pt/C electrocatalyst. The durability against start-stop and load potential cycling was successfully improved compared with the reference catalysts, as verified by half-cell voltammetry and full membrane-electrode-assembly (MEA) tests. Durability against start-stop cycling was attributed to the use of a thermochemically-stable TaO_x support which prevents direct contact between Pt and MC, thus minimizing carbon corrosion. Durability against load cycling was mainly attributed to the mesoporous structure, preventing the agglomeration of Pt catalyst particles. As such, the Pt/TaO_x/MC cathode electrocatalysts presented in this work have the potential to achieve both high durability and high power output, which is especially attractive for heavy-duty vehicular fuel cell applications.

1. Introduction

The climate crisis is driven by greenhouse gas emissions originating from the burning of fossil fuels. Global heating is an urgent global issue, and many nations have declared their intention to achieve carbon neutrality by 2050. More than 150 countries or regions have announced their commitment to decarbonization, whilst renewable energy is being rapidly implemented across societies around the world [1,2]. However, the issues of intermittency and energy storage remain to be solved at scale. Hydrogen is a chemical secondary energy carrier that can be produced from a variety of industrial processes and does not emit carbon dioxide at the point of utilization. As such, it is expected that hydrogen will be widely applied in the transportation, industry, and power generation sectors [3–7].

A core technology in hydrogen utilization is the polymer electrolyte fuel cell (PEFC). PEFCs convert the chemical energy of hydrogen into a voltage, and are already being applied to power fuel cell electric vehicles (FCEVs) in the transportation sector. They are already being applied in heavy-duty vehicles (HDVs) including as trucks, buses, trains, ships, and even airplanes to help realize zero emission mobility [5–10]. However, the effective use of PEFCs as a power source for HDVs requires higher power output and much greater durability than currently acceptable for e.g. passenger vehicles, with estimated improvements of around three and six times required, respectively [11,12]. PEFCs have already been largely optimized using the materials currently available, so further improvements can only feasibly be achieved by the development of innovative materials and cell architectures. Currently, cathode electrocatalysts exhibit particularly high overvoltages despite the use of highly active platinum-cobalt alloy nanoparticle catalysts, which accounts for a large fraction of the total capital expenditure of PEFC stacks. Therefore, the development of alternative electrocatalysts which simultaneously achieve higher catalytic activity and improved durability is imperative.

The structure of the electrocatalyst layer in PEFCs is highly complex and contains multiple materials and phases. They generally comprise of electrocatalyst nanoparticles decorated on a porous carbon support such as carbon black (for improvement of electron conduction and surface area), coated with a thin ionomer layer (for proton transport). However, PEFC cathodes operate in a severe environment, reaching high

* Corresponding author. Department of Hydrogen Energy Systems, Faculty of Engineering, Kyushu University, Motooka 744, Nishi-ku, Fukuoka, 819-0395, Japan.
E-mail address: sasaki@mech.kyushu-u.ac.jp (K. Sasaki).

https://doi.org/10.1016/j.ijhydene.2024.05.396
Received 16 March 2024; Received in revised form 23 May 2024; Accepted 26 May 2024
Available online 3 June 2024

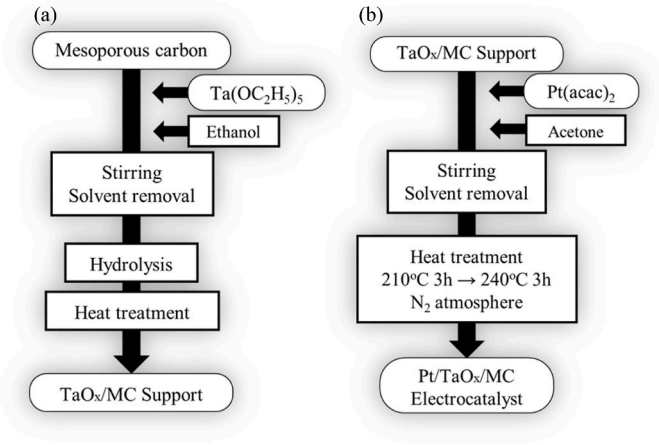

Fig. 1. Protocol for (a) synthesis of the TaOx/MC support, and (b) decoration of the support with platinum nanoparticles using the acetylacetonate (acac) complex method.

Table 1
Start-stop cycle durability test conditions [63].

Cell temperature	80 °C
Flow rate	Anode: H_2, 70 cc min^{-1} | Cathode: N_2, 166 cc min^{-1}
Maximum potential	1.5 V
Minimum potential	1.0 V
Rate of potential change	500 mV s^{-1}
Number of cycles	Up to 60,000 cycles, with ECSA measurements and performance tests after 1k, 2k, 5k, 10k, and 30k cycles.

Table 2
Load cycle durability test conditions [63].

Cell **temperature**	80 °C
Flow rate	Anode: H_2, 70 cc min^{-1} | Cathode: N_2, 166 cc min^{-1}
Maximum potential	0.95 V
Minimum potential	0.6 V
Time of each potential step	6 s
Number of cycles	Up to 100,000 cycles, with ECSA measurements and performance tests after 1k, 3k, 5k, 10k, 20k, 50k and 100k cycles.

temperatures (e.g. 80 °C), in strongly acidic conditions (~pH = 0), and widely fluctuating potentials. In particular, in FCEVs (including HDVs), the electrocatalyst is frequently subjected to potential fluctuations associated with start-stop and acceleration/deceleration load cycling, which accelerates degradation via two main mechanisms [8,13–17].

The first important degradation mechanism is oxidative corrosion of the carbon support during start-stop potential cycles. Thermochemically, the equilibrium potential of carbon oxidation is 0.207 V. However, in real-world environments, it has been reported that oxidative corrosion can progress rapidly when the potential reaches values such as 1.0–1.1 V versus the reversible hydrogen electrode (RHE) [14]. It is known that the cathode potential can temporarily rise to almost 1.5 V during gas displacement inside the stack when the fuel cell is switched on and off, resulting in the gradual oxidization over the lifetime of the device [13–17]. This carbon corrosion can result in electrocatalyst particle detachment from the support resulting in a decrease in the electrochemical surface area (ECSA), and a decrease in electronic conductance resulting in an increase in electrode resistance. These effects lead to an increase in overvoltage, ultimately leading to a decrease in PEFC power output and efficiency.

A huge number of studies have attempted solve the issue of carbon corrosion. For example, alternative carbon materials with higher corrosion resistance and larger surface area have been investigated, including graphitized carbon black [18–20]; graphitized carbon fibers [21]; carbon nanotubes (CNTs) [22,23]; mesoporous carbon (MC) [24,25]; graphene [26,27]; and related materials such as nitrogen-doped carbon [27–29]. Despite some reported improvements, electrochemical oxidation in any carbon material is inevitable under the required conditions. As such, many studies have also been conducted on alternative catalyst supports, and especially those incorporating metal oxides [30,31]. Metal oxides are already oxidized by their nature, and therefore are generally resistant to further oxidation. As such, they can improve start-stop cycle durability by preventing direct contact between the Pt catalyst and the carbon material.

The extreme environment of a PEFC cathode means that suitable metal oxides which are stable under these conditions are limited [30,31]. To mention a few, materials such as titanium dioxide (TiO_2) [32,33], tungsten trioxide (WO_3) [34,35], molybdenum dioxide (MoO_2) [36], and niobium pentoxide (Nb_2O_5) [37] have been investigated as platinum supports. Tin dioxide (SnO_2) has attracted particular attention as a material with high stability and electronic conductivity under PEFC cathode conditions. Our research group has been investigating metal oxides as catalyst supports for two decades, including TiO_2 and SnO_2, which are stable even in strong acidity and high potential environment [38]. Furthermore, we have developed Nb-doped SnO_2 supports which display higher conductivity and durability relative to other metal oxides [31,39–44]. Other research groups are also developing alternative electrocatalysts using e.g. SnO_2 [45,46].

Another important degradation mechanism is the dissolution and redeposition of Pt catalysts under load potential cycling during PEFC operation. Especially for automobile applications, the voltage fluctuates frequently due to acceleration and deceleration of the vehicle, usually between 0.6 and 0.95 V vs. RHE. During these changes in potential, the Pt/PtO_x redox reaction takes place on the surface of catalyst nanoparticles, and it has been shown that Pt can dissolve at potentials above ca. 0.85 V in the cathode environment [8,30]. Furthermore, in this process, Pt particles with smaller diameters are oxidized to Pt^{2+} ions which dissolve in the acidic solution and are then reduced and re-deposited on the surface of more thermodynamically stable Pt particles with larger diameters, a process known as Ostwald ripening [47,48]. Increasing the catalyst particle size decreases surface area, leading to a decrease in mass activity (MA) and power output. Furthermore, potential fluctuations can also result in Pt particle aggregation due to particle mobility on the support surface [47,48]. Various efforts have been made to prevent these degradation mechanisms [49–51]. One common solution is to employ mesoporous carbon supports. Mesopores are classified as having diameters in the range of 2–50 nm. Because of the unique porous structures and often large surface area of MCs, many studies have explored their use as a catalyst support in PEFCs [8,24,25,52,53]. From the viewpoint of catalyst degradation, it has been reported that nanoparticles residing within mesopores do not have direct contact with the strongly acidic ionomers, suppressing Pt dissolution and thus improving load cycle durability [54,55]. Again, metal oxide supports are beneficial in the minimization of these issues, due to the strong interaction between the metallic catalyst and the metal oxide support, which suppresses dissolution and agglomeration of platinum nanoparticles [56].

Here, we aim to combine the benefits of using mesoporous carbons and the benefits of employing metal oxides to overcome the main degradation mechanisms of carbon corrosion and dissolution/agglomeration under start-stop and load cycling conditions. In this paper, we focus on tantalum oxides with a high melting point of 1875 °C [57], which are thermochemically stable in the strongly acidic environment of PEFC cathodes [30,31]. Only a limited number of studies have considered tantalum as a potential material for PEFC cathode electrocatalysts [31,58–60]. One of the drawbacks of using metal oxides in electrocatalyst layers is the relatively low electrical conductivity compared with carbon. As such, we attempt to potentially improve the

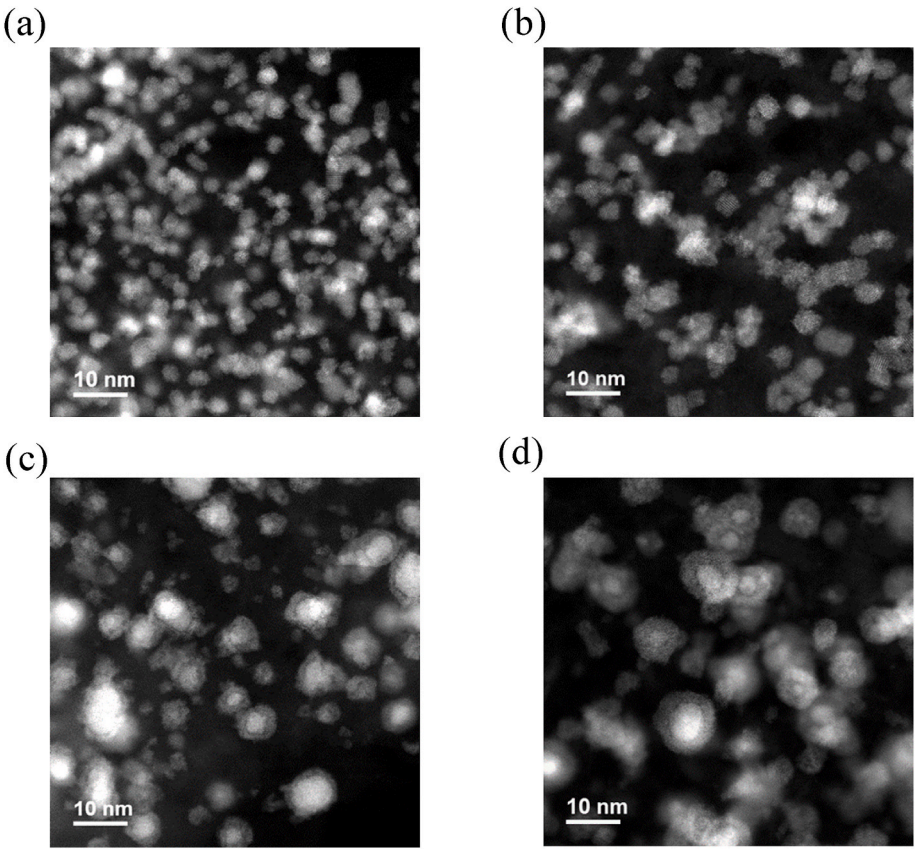

Fig. 2. STEM transmission images of the TaO_x/MC supports heat-treated in: H_2 at (a) 700 °C and (b) 800 °C; and in Ar at (c) 1300 °C and (d) 1400 °C. TaO_x particles stand out in bright contrast.

conductivity of tantalum oxide by partial reduction from Ta_2O_5 to nonstoichiometric TaO_x. The preparation and evaluation of Pt/TaO_x/MC electrocatalysts will open up new possibilities for improved performance and durability in PEFCs.

2. Experimental

2.1. Preparation of the TaO_x/MC supports

The support synthesis procedure is summarized in Fig. 1a. Tantalum ethoxide ($Ta_2(OC_2H_5)_5$, Kojundo Chemical Laboratory Co., Ltd., Japan) was dissolved in ethanol (Kishida Chemical Co., Ltd., Japan), and then mesoporous carbon (CNovel® MJ(4)010, Toyo Tanso, Co., Ltd., Japan, nominal pore diameter 10 nm) was dispersed in this solution. Tantalum ethoxide was added such that the ratio of tantalum to mesoporous carbon was 35 wt %. The resulting dispersion was dried under reduced pressure using a rotary evaporator (SE-1000, Eyela, Japan), a vacuum pump (EVP-1000, Eyela, Japan), and a pressure controller (NVC-2300A, Eyela, Japan), whilst simultaneously applying ultrasonic agitation (MCS-3P, AS ONE, Japan) until all the solvent was evaporated. Then, steam hydrolysis was conducted by supplying 3%-humidified N_2 gas at room temperature for 1 h. After this, the powder was first heated at 400 °C for 2 h, then at 800 °C for 30 min, in inert gas (either N_2 for subsequent H_2 treatment, or Ar for subsequent Ar treatment). The resulting powder was then heated either under flowing hydrogen gas at between 500 °C and 800 °C for 2 h, or under flowing argon gas at between 800 °C and 1400 °C for 2 h, to partially reduce the Ta_2O_5 to TaO_x. This resulted in tantalum oxide-coated mesoporous carbon (TaO_x/MC) powders.

2.2. Preparation of the Pt/TaO_x/MC electrocatalysts

Subsequently, the TaO_x/MC supports were decorated with Pt catalyst nanoparticles using the acetylacetonate (acac) method (Fig. 1b) [24]. First, Pt acetylacetonate (Sigma-Aldrich Co., LLC, USA) was dissolved in acetone (Kishida Chemical Co., Ltd., Japan), and then the TaO_x/MC support powder was dispersed in this solution. The dispersion was then dried using the rotary evaporator under ultrasonic agitation until all the solvents was evaporated. The obtained powder was then heat-treated at 210 °C for 3 h and then at 240 °C for 3 h under flowing nitrogen gas, reducing the platinum precursor to platinum metal. This procedure resulted in the formation of Pt/TaO_x/MC electrocatalyst powders. Platinum-decorated mesoporous carbon (Pt/MC) was also prepared by the same procedure as a reference sample. The Pt loading in both cases was set to be 30 wt%.

2.3. Microstructural characterization of the supports and electrocatalysts

The microstructure of the resulting supports and electrocatalysts was observed using high-resolution field-emission scanning electron microscope (FE-SEM, SU9000, Hitachi High-Tech Corporation, Japan) and scanning transmission electron microscope (STEM, JEM-ARM200F, JEOL Ltd., Japan) coupled with energy dispersive X-ray spectroscopy (EDS). The crystalline state of the TaO_x/MC supports was evaluated via X-ray diffractometry (XRD, RINT Ultima III, Rigaku, Japan). The pore size distribution was measured using a high-precision gas adsorption system (BELSORP-mini–II–SP, MicrotracBEL, Japan).

2.4. Electrochemical characterization of the electrocatalysts

Electrochemical measurements were first performed using a rotating

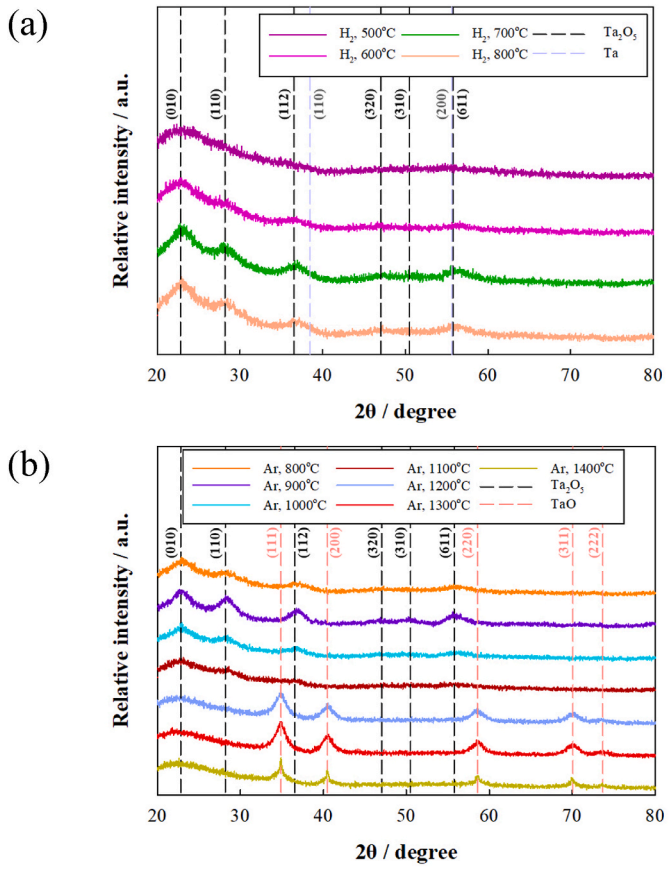

Fig. 3. XRD spectra of TaO_x/MC supports heat treated in (a) H_2 and (b) Ar at various temperatures. Dashed lines indicate the peak positions with their indices of Ta_2O_5 and Ta in (a), and Ta_2O_5 and TaO in (b).

disk electrode system (RDE, HZ-5000, Hokuto Denko Corp., Japan). Electrocatalyst ink comprising the electrocatalyst powder, 2-propanol (Wako Pure Chemical Industries, Ltd., Japan), ultrapure water (18.2 MΩ, Direct-Q UV5, Merck Millipore), and 5% Nafion solution (Wako Pure Chemical Industries, Ltd., Japan) was prepared by stirring with an ultrasonic homogenizer (UH-600, SMT Co., Ltd., Japan). To prepare the working electrode, each electrocatalyst ink was carefully deposited onto a glassy carbon (GC) disk electrode with an electrode area of 0.196 cm^2, with a fixed platinum loading of 17.3 $\mu g_{\text{-Pt}}$ cm^{-2} [61]. Cyclic voltammetry (CV) was performed under static conditions in N_2-saturated 0.1 M $HClO_4$ at 25 °C. The scanning rate was 50 mV s^{-1} and the scanning range was 0.05–1.2 V_{RHE} [62]. The electrochemical surface area (ECSA) of Pt after 50 potential cycles was derived from the hydrogen desorption region (0.05–0.4 V_{RHE}) of the obtained CV curves. The linear sweep voltammograms (LSVs) were used to evaluate the oxygen reduction reaction (ORR) activity via RDE measurements performed in O_2-saturated 0.1 M $HClO_4$ at 25 °C, at a scanning rate of 10 mV s^{-1} in a range of 0.2–1.2 V_{RHE}, with an electrode rotation speed varying from 2500 to 400 rpm. The mass activity (MA, i.e. the current per unit mass of Pt) was calculated at 0.9 V_{RHE}.

Meanwhile, the durability of the electrocatalysts was evaluated by applying potential cycles simulating the load cycles of a real-world system according to protocols recommended by the New Energy and Industrial Technology Development Organization (NEDO) [63]. Load cycling (which accelerates Pt dissolution and re-deposition) was performed for 100,000 cycles with a square potential wave between 0.6 and 0.95 V_{RHE} with 6 s per cycle. The ECSA was measured periodically during the durability tests.

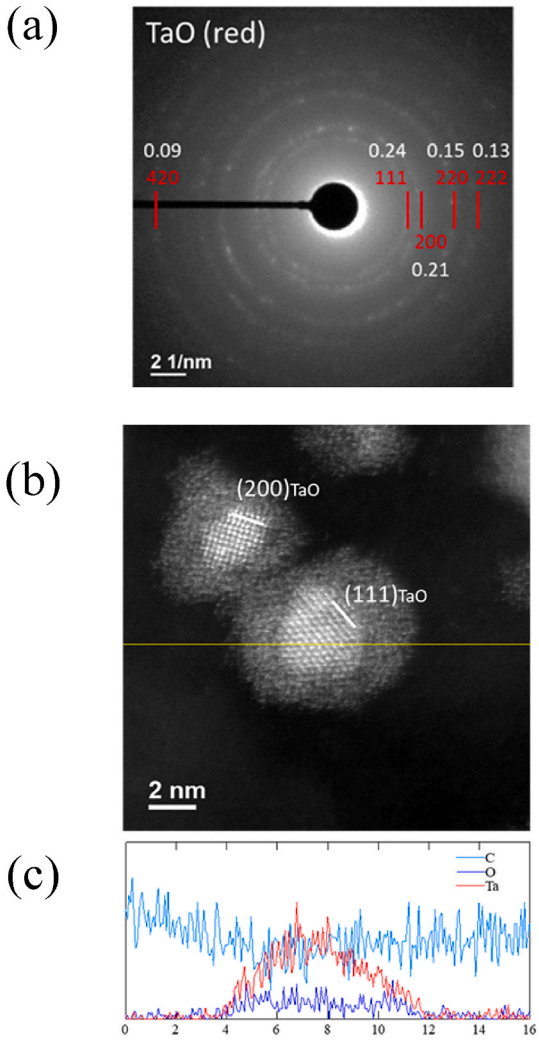

Fig. 4. (a) Selected area electron diffraction pattern; (b) STEM-EDS line analysis; and (c) elemental distribution of C, O, and Ta for the TaO_x/MC support treated in Ar at 1300 °C.

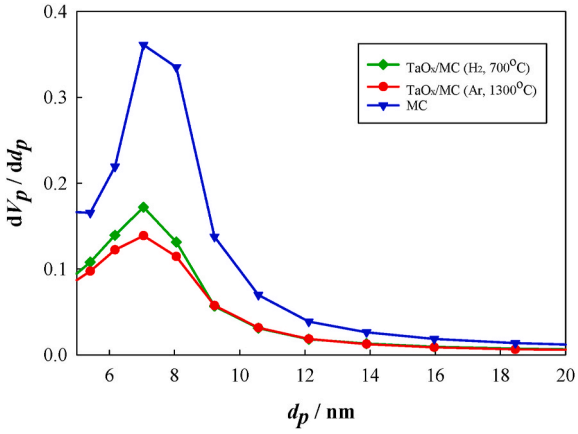

Fig. 5. Barrett-Joyner-Halenda (BJH) pore size distribution of selected electrocatalyst supports.

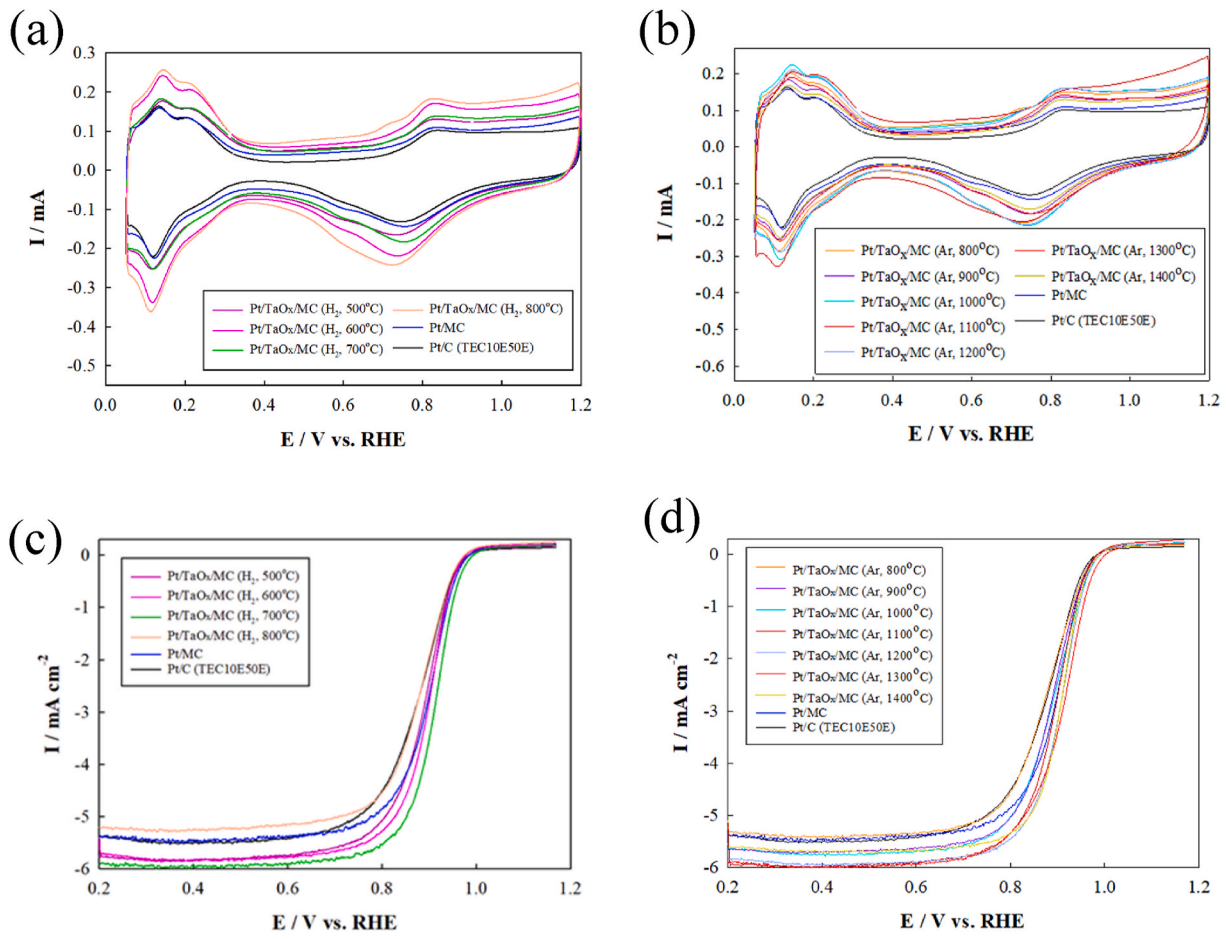

Fig. 6. (a, b) CV spectra and (c, d) LSV curves comparing Pt/TaO_x/MC electrocatalysts, treated in (a, c) H_2 and (b, d) Ar, at various temperatures. The data for Pt/MC and Pt/C are also shown for comparison.

2.5. Preparation of membrane electrode assemblies (MEAs)

Electrocatalyst paste was prepared by dispersing the Pt/TaO_x/MC electrocatalyst powder (or a reference Pt-decorated Ketjenblack electrocatalyst, 46.4 wt% Pt, TEC10E50E, Tanaka Kikinzoku Kogyo K.K., Japan), 99.5% ethanol, ultra-pure water, and 5 % Nafion solution, using the ultrasonic homogenizer. This electrocatalyst paste was then sprayed onto an electrolyte membrane (Nafion 212, Chemours Co., Delaware, USA) using a spray printing system (C-3 J, Nordson Co., USA). The electrode area was 1.0 cm^2 (1 cm × 1 cm). The Pt/TaO_x/MC electrocatalysts were applied to the cathode with a Pt loading of 0.2 $mg_{\cdot Pt}$ cm^{-2}; a Nafion content of 28 wt % (ionomer/carbon ratio, I/C = 0.83); and a solids ratio for spray printing of 4 wt % (obtained by mixing ultra-pure water and ethanol in a volume ratio of 1:9). For the anode, the Pt/C (TEC10E50E) was used as the electrocatalyst; the Pt loading was set to be 0.1 $mg_{\cdot Pt}$ cm^{-2}; the Nafion content was also 28 wt % (but with I/C = 0.73), and the solids ratio was 3.5 wt %.

After spray printing, the MEAs were prepared by hot-pressing at 132 °C and 0.3 kN for 180 s. Finally, both electrodes were sandwiched between two hydrophobic gas diffusion layers (GDLs). The cathode GDL was coated with a microporous layer (22BB, SGL Carbon GmbH, Germany) and the anode GDL was uncoated (EC-TP1-060T, Electrochem Inc. USA). The PTFE-based sealant thickness was 100 μm on the cathode side and 180 μm on the anode side. The Nafion content and sealant thickness have been previously optimized for improved cell performance [64].

2.6. Evaluation of MEAs

Current-voltage (I–V) characteristics of MEAs were evaluated at 80 °C and 100% relative humidity (RH). The cell temperature and the gas humidification temperature were both set at 80 °C, and the gas utilization of air and H_2 was set to be 2% at 1 A cm^{-2} for both the cathode and the anode. During MEA measurements, the gas pressure was set to be 1.5 bar. A fuel cell evaluation system (AutoPEM-TH042B, Toyo Co., Japan) was used for cell performance measurements. A cell holder, with three serpentine-shaped gas flow channels, was used for the evaluation of MEAs with 1 cm^2 electrodes, as developed in a NEDO project. Before I–V measurements, MEAs were pre-treated at 0.6 V for 4 h. At each step of measurement (18 steps between 0.95 V and 0.2 V), the cell voltage was held constant for 5 min, and the current density averaged over the final minute was recorded. For evaluating the various overvoltages, the ohmic cell resistance was measured using an AC impedance analyzer (SP-240 Potentiostat, BioLogic, France), and the IR loss was separated by subtracting the ohmic contribution (IR loss) from the recorded cell voltage. The IR-free voltage loss was then separated into activation overvoltage and concentration overvoltage. A Tafel plot was created with current density plotted on the logarithmic x-axis, and the IR-free cell voltage plotted on the y-axis. In the low current density region, 3 to 4 values were fitted with linear regression. The difference between the theoretical electromotive force (1.17 V at 80 °C for an H_2/air cell at ambient pressure) and the voltage of the linear regression line was taken as the activation overvoltage at the current density of interest. The deviation of the IR-free voltage from the voltage at the linear regression line in the Tafel plot was taken as the concentration

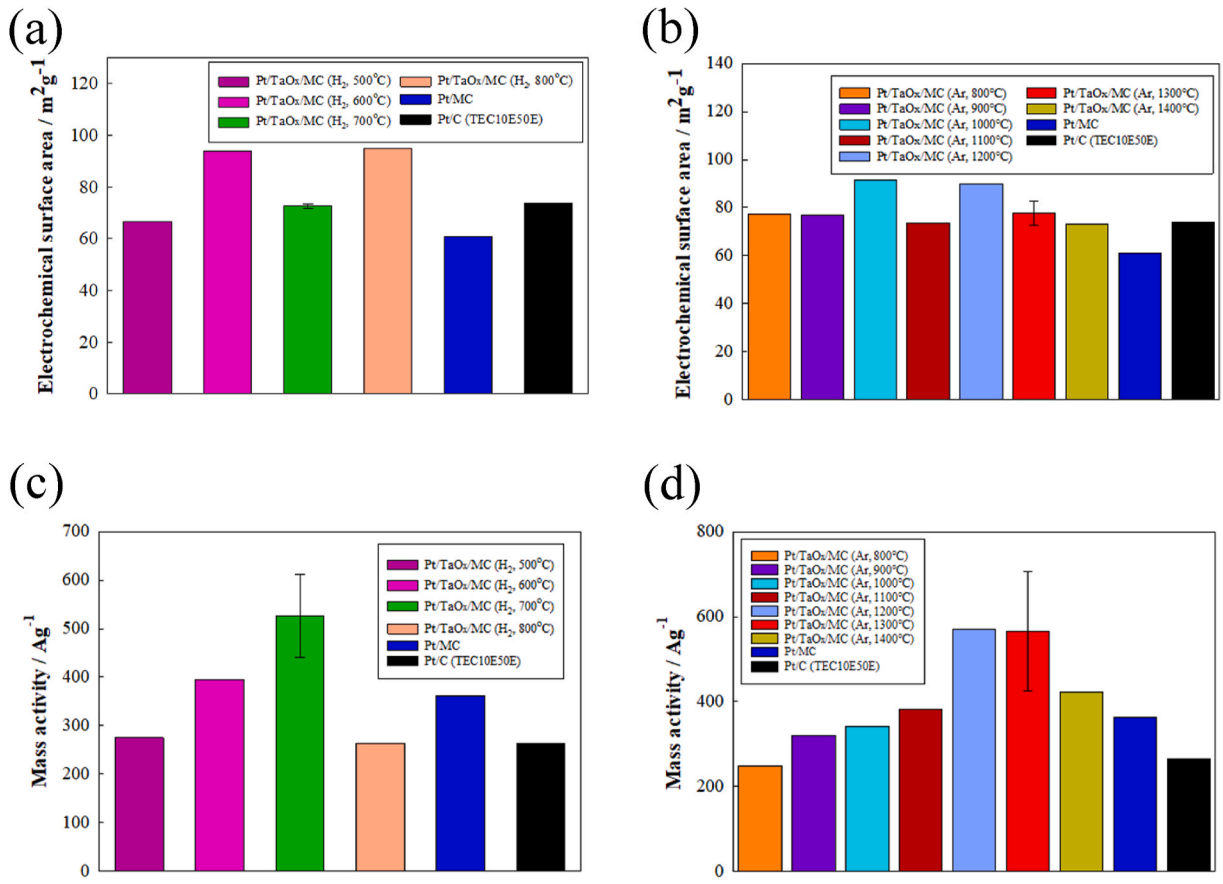

Fig. 7. (a, b) ECSA and (c, d) MA at 0.9 V_{RHE} for Pt/TaO_x/MC electrocatalysts, heat treated in (a, c) H_2 and (b, d) Ar, at various temperatures. The data for Pt/MC and Pt/C are also shown for comparison.

overvoltage [63]. Cross-sectional micrographs of the electrocatalyst layers were taken by using a focused ion beam scanning electron microscope (FIB-SEM, Helios NanoLab 600i, FEI) to evaluate their thickness.

To evaluate the durability of MEAs, accelerated degradation tests were performed. A protocol simulating the start-stop cycles and load cycles of FCEVs were used, as recommended by the NEDO [63]. According to this protocol, the start-stop potential cycle comprises a triangular potential waveform between 1.0 and 1.5 V, with 2 s per cycle. The start-stop cycles simulate the fuel cell start-stop operation, accelerating carbon corrosion. The load potential cycle comprises a square potential waveform between 0.6 V and 0.95 V, with 6 s per cycle. This load cycle simulates output fluctuations due to acceleration and deceleration. The detail conditions of the start-stop cycle durability test and the load cycle durability test are shown in Tables 1 and 2, respectively. It has been reported that load cycle durability tests up to 30,000 cycles corresponds to a real-world driving range of 200,000 km over 6000 h [65], which is the lifetime of a typical passenger vehicle [8].

3. Results and discussion

3.1. Characterization of the TaO_x/MC supports

Representative STEM transmission images of the TaO_x/MC catalyst supports heat-treated (a) in H_2 at 700 °C; (b) in H_2 at 800 °C; (c) in Ar at 1300 °C; and (d) in Ar at 1400 °C are shown in Fig. 2. Ta-rich phases stand out in bright contrast due to their relatively higher atomic mass compared to carbon. In (a), they are observed to have diameters of a few nanometers, and are highly dispersed throughout the mesoporous carbon support. This suggests that the unchecked growth of Ta-based grains is suppressed, due to confinement within the MC mesopores. However, in (b), the Ta-rich phase grains are observed to be more aggregated. This is attributed to the higher temperature, resulting in possible gasification of the carbon via reaction with hydrogen to form methane, losing the confinement effect of mesopores. In (c), slightly larger but well-dispersed tantalum-rich phases are still observed despite the higher temperature, attributed to the inert gas used in this case, preventing gasification of the mesoporous carbon. However, in (d), again agglomeration of the tantalum-rich phases is observed, attributed to the higher temperature of 1400 °C affecting the carbon structure.

Fig. 3a shows the XRD patterns of supports heat-treated in hydrogen gas at 500, 600, 700, and 800 °C. Fig. 3 also shows the XRD peak positions of Ta_2O_5, TaO, and Ta. As the temperature increases, peaks corresponding to Ta_2O_5 appear. However, in (a), no XRD peaks are observed for metallic Ta and TaO phases, suggesting that the tantalum oxide is not fully reduced to its metallic phase or the TaO phase even in the strongly reducing conditions of hydrogen gas at 800 °C. It may be possible that 800 °C was still too low to reduce the relatively thermostable Ta_2O_5 to TaO or Ta due to the high melting point of Ta_2O_5, even in hydrogen gas. Meanwhile, Fig. 3b shows the XRD patterns after heat treatment in argon gas between 800 °C and 1400 °C. In this case, the crystallinity increases up to 900 °C, but then the intensity of the Ta_2O_5 peak decreases at higher temperatures of 1000 °C and 1100 °C. Formation of oxygen-deficient tantalum oxide (TaO) is confirmed after heat treatment at 1200, 1300, and 1400 °C (highlighted by the pink dotted lines).

Fig. 4 shows (a) selected area electron diffraction, (b) STEM-EDS line analysis, and (c) elemental distribution (C, O, and Ta) of the TaO_x/MC support heat-treated in Ar at 1300 °C. The diffraction rings corresponding to TaO_x are denoted in red (Fig. 4a) and confirm the reduction

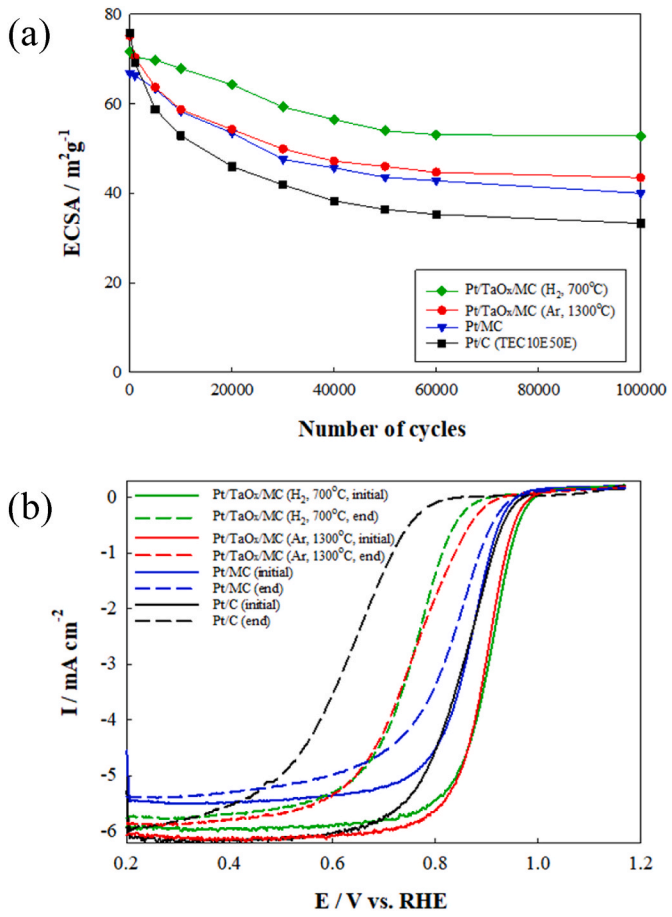

Fig. 8. (a) ECSA of selected electrocatalysts during load cycle durability tests, and (b) LSV (1600 rpm) before (initial) and after (end) the load cycle durability tests, both measured in half-cell tests.

of Ta_2O_5 to the partially-reduced form, TaO. In addition, crystalline planes corresponding to TaO are clearly observed in Fig. 4b. Furthermore, Fig. 4c shows line scans of each element, indicating that the degree of oxidation is different between the center of the tantalum-based particles and their surface, with the center being more reduced (i.e., $x < 1$) and the surface being less reduced (i.e., $x \geq 1$). It may be possible that MC acts as a reducing agent, reducing Ta_2O_5 to TaO_x even in Ar, which is an inert gas.

The pore size distribution of the support materials was also measured using the Barrett-Joyner-Halenda (BJH) gas adsorption method as shown in Fig. 5. The mode mesopore diameter of all of the MC-based supports was ~7 nm, but the mesopore volume decreased in the order of pure MC, to TaO_x/MC (H_2/700 °C), and to TaO_x/MC (Ar/1300 °C). It is concluded from this data that the TaO_x particles account for around half of the total mesopore volume of the samples. These results indicate that there remains available space for Pt catalyst decoration on the TaO_x support within the mesopores, but sufficient TaO_x is still available within the mesopores to act as a catalyst support.

3.2. Electrochemical characterization

CV curves (Fig. 6a and b) and LSV curves (Fig. 6c and d, measured at 1600 rpm) of the Pt/TaO_x/MC electrocatalysts are shown in Fig. 6. The catalyst supports heat-treated in hydrogen are represented in Fig. 6a and c, whilst those heat-treated in argon are shown in Fig. 6b and d. The data for Pt/MC and Pt/C (TEC10E50E) electrocatalysts are also shown for comparison. Meanwhile, the ECSA values derived from the CV curves are shown in Fig. 7a and b, while the MA values derived from the LSV curves are shown in Fig. 7c and d, also separated into heat treatment in hydrogen or argon. There are no major changes in the profiles of the CV curves associated with the addition of tantalum oxide compared with the pure carbon supports, and the ECSA values all fall in the range of 60 to ca. 90 $m^2\ g^{-1}$ for all the electrocatalysts studied here. In contrast, there is a clear positive shift in the LSV curves as the heat treatment temperature increases for both H_2 and Ar heat treatments (Fig. 6c and d). Fig. 7 clearly reveals that the highest MA was observed after heat treatment in hydrogen at 700 °C, and after heat treatment in argon at 1200 °C and 1300 °C, all exceeding 500 A g^{-1}, which is twice as high as the recorded values of the commercial Pt/C reference electrocatalyst with an MA of around 250 A g^{-1}.

Possible reasons for this increase in MA include the likely higher electrical conductivity of nonstoichiometric TaO_x relative to Ta_2O_5, surface defects on TaO_x, and/or a strong Pt-TaO_x interaction after the high temperature treatment steps. Spillover effects on the Pt-TaO_x surface, strong acidity of TaO_x, oxygen vacancy on oxygen-deficient TaO_x, structural stability of Pt with TaO_x, and/or a strong electronic metal-oxide interaction affecting electronic state of Pt catalysts [58,59] could also be related for improved oxygen reduction reaction (ORR) activities. In contrast, a decrease in MA was observed when the heat treatment temperature raised further to either 800 °C in hydrogen or 1400 °C in Ar. This is attributed to the significant change in microstructure of the carbon, and large grain size of tantalum-based phases observed in these samples, as observed by STEM (Fig. 2b and d).

3.3. Load cycling durability

The catalysts based on supports heat-treated in hydrogen at 700 °C or in argon at 1300 °C which displayed high MA were additionally subjected to half-cell load cycle durability tests. The changes in ECSA throughout the test, and LSV curves before and after the durability tests are shown in Fig. 8. Both Pt/TaO_x/MC electrocatalysts displayed improved load cycle durability, with a relatively gradual decrease in ECSA (Fig. 8a) and an excellent retention of ORR activity (Fig. 8b) compared to the standard Pt/C electrocatalysts. The values of ECSA retention in the two Pt/TaO_x/MC electrocatalysts were 74% and 58%, respectively (Fig. 8a). This is attributed to the use of MC as the catalyst support framework, preventing catalyst migration/aggregation due to Pt confinement in mesopores as well as the strong metal support interaction between platinum and TaO_x, further preventing dissolution and migration. However, in the case of the LSVs, the Pt/MC electrocatalyst retained its ORR activity to a greater degree than the Pt/TaO_x/MC electrocatalyst. A possible explanation for this is that the TaO_x particles become more oxidized throughout the long-term durability test, probably returning to their less electronically conductive Ta_2O_5 phase.

Detailed microstructural images of the Pt/TaO_x/MC electrocatalysts treated in H_2 at 700 °C and in Ar at 1300 °C before and after the load cycle tests are shown in Fig. 9. STEM-EDS maps (Fig. 9a and b) show that the grain size of the initial Pt particles (green) was ca. 2–3 nm diameter before the load cycle tests. In contrast, after the load cycle tests, a proportion of the Pt particles have grown to larger than 10 nm in diameter, while others still remain small at ~5 nm (Fig. 9c and d). Little aggregation is observed and this is attributed to suppressed migration of platinum catalyst on the metal oxide support and in the carbon mesopores. Furthermore, transmission STEM images (Fig. 9e and f) show that the Pt particles on the surface of the MC grains (denoted with red circles with dashed lines) are coarsened. However, the Pt particles within the MC grains maintained their (small) size, thus indicating that aggregation of Pt particles within mesopores is suppressed. The Pt particles on the surface of the MC grains tended to be larger, especially in the electrocatalyst heat-treated in Ar at 1300 °C, suggesting that a larger proportion of Pt was deposited outside the mesopores compared with the electrocatalyst heat-treated in H_2 at 700 °C. Crucially, it is desirable for Pt catalysts to be decorated within the mesopores to ensure a higher load cycle durability.

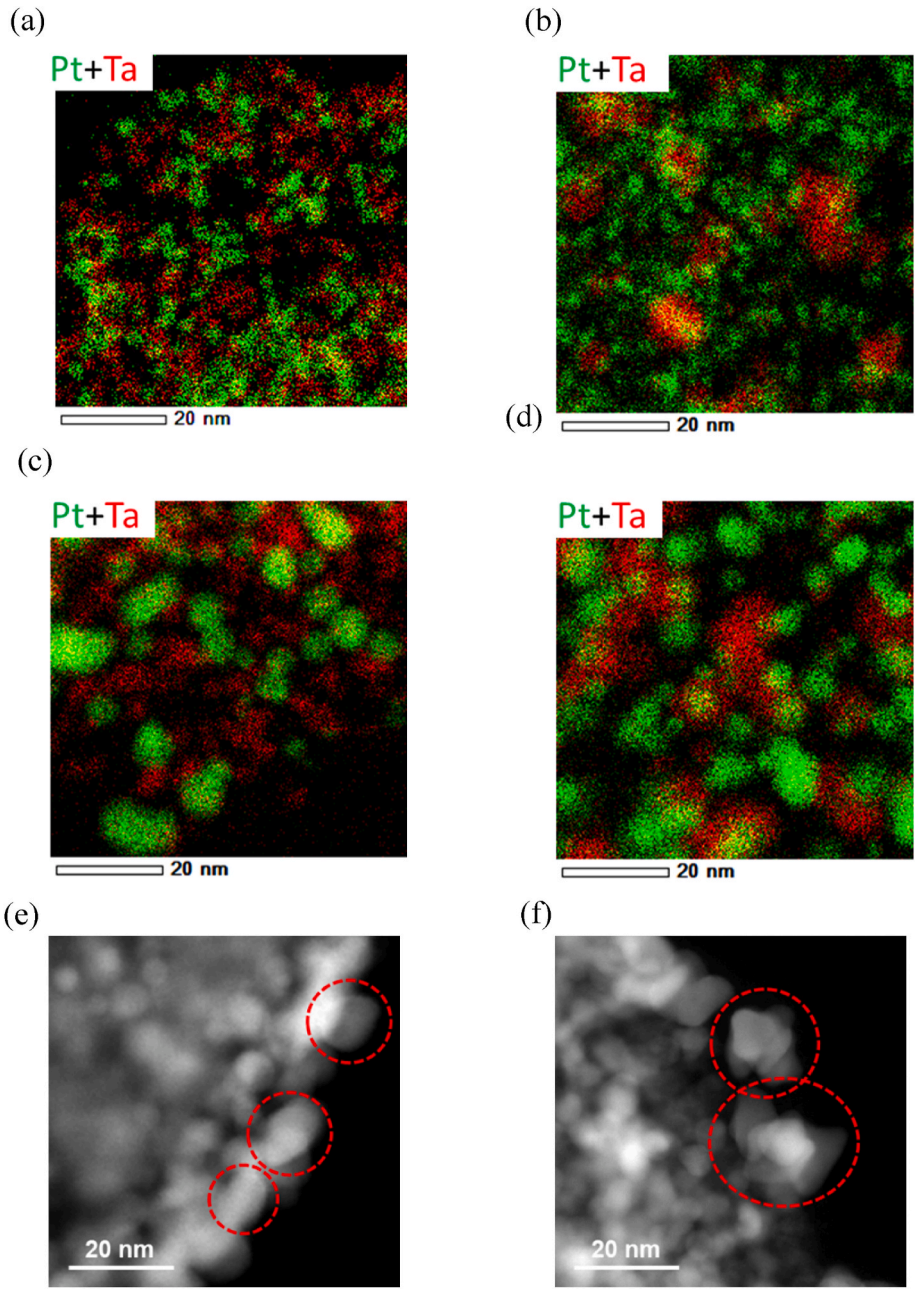

Fig. 9. (a–d) STEM-EDS maps of Pt (green) and Ta (red) and (g, h) STEM images of the Pt/TaO_x/MC electrocatalysts, treated (a, c, e) in H_2 at 700 °C and (b, d, f) in Ar at 1300 °C, (a, b) before and (c–f) after the load cycle tests. In (e) and (f), Pt catalyst nanoparticles are aggregated on the MC grain surface denoted with red circles with dashed line, while other nanoparticles within the MC grains remain smaller. (For interpretation of the references to colour in this figure legend, the reader is referred to the Web version of this article.)

3.4. Electrochemical performance of MEAs

Fig. 10a shows the I–V characteristics of an MEA using the best-performing Pt/TaO_x/MC electrocatalyst, namely that heat-treated at 1300 °C in Ar. The corresponding I–V curves for the Pt/MC and Pt/C (TEC10E50E) reference samples are also shown for comparison. Overall, the cell performance with the Pt/TaO_x/MC electrocatalyst is slightly lower than for the Pt/C reference, but still displays sufficiently high cell voltage up to relatively high current densities beyond 3 A cm^{-2}. Fig. 10b, 10c, 10d, and 10e show the power density, the activation overvoltage, the IR loss, and concentration overvoltage, respectively. The power density of the MEA with the Pt/TaO_x/MC electrocatalyst was comparable to that with the reference Pt/C (Fig. 10b). The activation overvoltage (Fig. 10c) was similar for all three fabricated cells. To further reduce the activation overvoltage, it is necessary to increase the utilization of platinum, especially in the low current density range. Furthermore, no difference in IR loss was observed (Fig. 10d) between the Pt/TaO_x/MC cell and the Pt/MC cell, indicating that the presence of TaO_x does not inhibit electrical conduction in the electrocatalyst layer (the specific electrical conductivity of TaO_x should be quantitatively evaluated in a future study). Fig. 10e shows that the concentration overvoltage is comparable between the Pt/TaO_x/MC cell and the Pt/C cell, leading to the excellent cell performance in the high current density region [66]. The thickness of the Pt/TaO_x/MC, Pt/MC, and Pt/C electrocatalyst layers were 6.9 ± 0.5 μm, 12.4 ± 0.5 μm, and 3.2 ± 0.2 μm, respectively, derived from 10 images of the FIB-SEM cross-sectional micrographs of each electrocatalyst layer. Since a Pt loading was set to be 30 wt% relative to the total mass of the support (TaO_x/MC for the

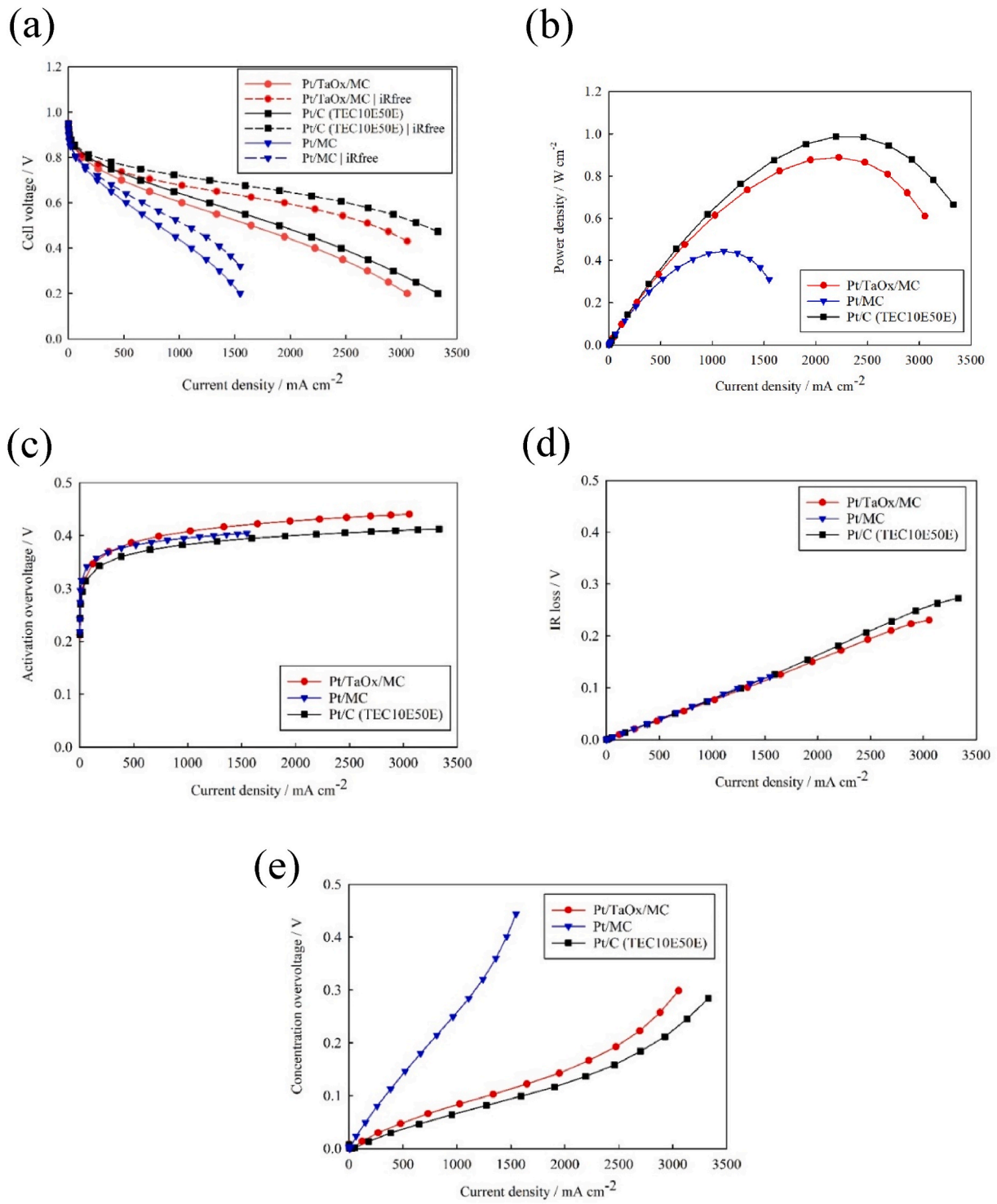

Fig. 10. Cell performance and overvoltages in using each electrocatalyst: (a) IV curve, (b) power density, (c) activation overvoltage, (d) IR loss, and (e) concentration overvoltage.

$Pt/TaO_x/MC$ electrocatalyst, and MC for the Pt/MC electrocatalyst), the Pt loading versus the mass of MC alone was consequently much higher for $Pt/TaO_x/MC$ than for Pt/MC, leading to a much thicker electrocatalyst layer for Pt/MC. The significant increase in concentration overvoltage of the Pt/MC cell (Fig. 10e) is likely attributed to this fact, resulting in less effective mass (O_2 and water) transport. The slightly lower current-voltage characteristics of the $Pt/TaO_x/MC$ cell compared to those of the Pt/C cell are attributed to a relatively inhomogeneous MC microstructure for $Pt/TaO_x/MC$ with a particle size distribution ranging from ~0.5 μm to 2 μm. Further optimization of this microstructure as well as the I/C ratio may be required to further improve the cell performance.

3.5. *Start-stop cycle durability of MEAs*

The durability against start-stop cycling of the MEAs using the $Pt/TaO_x/MC$ electrocatalyst heat-treated in Ar at 1300 °C, the Pt/MC electrocatalyst, and the Pt/C electrocatalyst was also evaluated at the

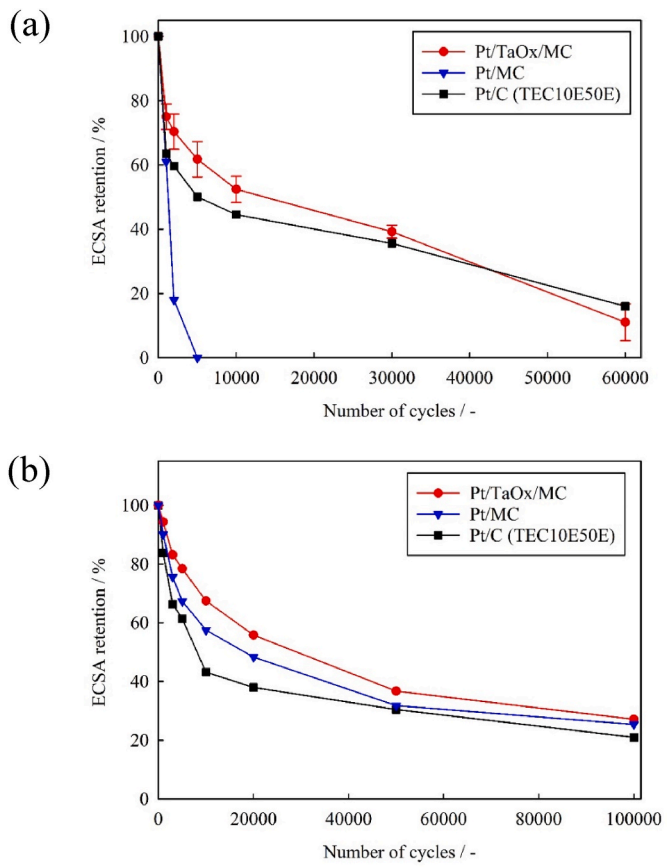

Fig. 11. ECSA retention of the cells using each electrocatalyst, (a) during 60,000 start-stop cycles and (b) during 100,000 load cycles.

full-cell level by applying 60,000 start-stop potential cycles. The ECSA (Fig. 11a) of the cell using Pt/MC decreased rapidly and approached zero after only 5000 cycles. In contrast, the cell with the Pt/TaO_x/MC electrocatalyst maintained an ECSA of ~10% even after 60,000 cycles. Whilst mesoporous carbon is not sufficiently durable against oxidative start-stop potential cycles, it is evident that the applying a TaO_x layer on the surface of mesoporous carbons can significantly improve the start-stop cycle durability by preventing the direct contact between the Pt catalyst and the carbon-based MC, as previously reported for SnO_2-based electrocatalyst supports [42–44]. The start-stop cycle durability of the cell using the Pt/TaO_x/MC electrocatalyst is comparable to that of the commercially available Pt/C reference, but this durability against start-stop cycles is expected to be further improved by optimizing e.g. the loading and distribution of TaO_x, the platinum loading, and the microstructure of the mesoporous carbon.

3.6. Load cycle durability of MEAs

The durability against load cycling of the MEAs was also evaluated at the full-cell level by applying 100,000 load potential cycles. The retention of ECSA for the Pt/TaO_x/MC cell was ~25% after 100,000 cycles, and in this case it was actually higher compared to both the Pt/MC and Pt/C references. The mesoporous carbons had improved retention in this case attributed to the prevention of aggregation of Pt particles confined in the mesopores, and the highest retention for Pt/TaO_x/MC is attributed to the further effect of the strong metal-support interaction between platinum and the tantalum oxide in addition to the mesopore effect. As such, both half-cell (Fig. 8a) and full-cell (Fig. 11b) results highlight the common trends that the use of mesoporous carbon in combination with tantalum oxide improves the load cycle durability, while the carbon black support (i.e. Ketjenblack) of the reference Pt/C sample contains micropores (i.e. < 2 nm) with a high surface area, ensuring a certain degree of load cycle durability. In future studies aiming to achieve both higher performance and durability, the mesoporous carbon should be further optimized by controlling the mesopore size and the degree of graphitization, whilst the TaO_x should also be optimized by controlling the TaO_x loading and distribution on the mesoporous carbon support, and increasing the electrical conductivity by partial reduction and/or chemical doping. Since the physical and surface properties of such nonstoichiometric TaO_x nanoparticles have not yet been fully explored in the literature, electrical conductivity and surface defects of TaO_x, and the strong interaction between Pt and TaO_x are also important issues of scientific and technological interest. As such, future studies should clarify the role that TaO_x plays in the electrochemical performance of Pt/TaO_x/MC electrocatalysts.

4. Conclusions

Improved durability against start-stop and load cycles is needed for PEFCs to be applied in e.g. heavy-duty automotive applications, especially in terms of the cathode electrocatalysts. Therefore, we have developed Pt/TaO_x/MC electrocatalysts to combine the advantages of mesoporous carbons and metal oxides in preventing platinum dissolution, agglomeration, and carbon corrosion. The highest initial MA beyond 500 A g^{-1} was observed after heat treatment of the support at 700 °C in H_2 or 1300 °C in Ar, a value which is doubled compared with a conventional Pt/C electrocatalyst. The durability of the cathode electrocatalyst against start-stop and load cycles was successfully improved compared with the reference catalysts, as verified by half-cell voltammetry and full MEA tests. Improved start-stop cycle durability is attributed to the use of a TaO_x support, preventing the direct contact between Pt and MC, thus minimizing carbon corrosion. Meanwhile high load cycle durability is mainly attributed to the mesoporous structure, preventing aggregation of the Pt catalyst particles. Improvements in both types of durability are simultaneously fulfilled using these electrocatalysts. These results indicate that TaO_x-based electrocatalyst supports using MC have the potential to achieve both high durability and high power output for PEFCs, and could therefore be suited to heavy-duty vehicular fuel cell applications.

CRediT authorship contribution statement

R. Nishiizumi: Writing – original draft, Investigation, Data curation. **T. Ogawa:** Writing – original draft, Investigation, Data curation. **K. Sanami:** Investigation, Data curation. **M. Yasutake:** Writing – review & editing, Supervision, Investigation. **Z. Noda:** Validation, Supervision, Investigation, Data curation. **S.M. Lyth:** Writing – review & editing, Investigation. **M. Nishihara:** Writing – review & editing, Investigation. **J. Matsuda:** Writing – review & editing, Visualization, Validation, Investigation, Data curation. **K. Sasaki:** Writing – review & editing, Supervision, Project administration, Investigation, Funding acquisition.

Declaration of competing interest

The authors declare that they have no known competing financial interests or personal relationships that could have appeared to influence the work reported in this paper.

Acknowledgement

This paper is based on results obtained from a project, JPNP20003, commissioned by the New Energy and Industrial Technology Development Organization (NEDO).

References

[1] International Energy Agency. Net zero by 2050 - a roadmap for the global energy sector. https://www.iea.org/reports/net-zero-by-2050; 2021.

[2] Agency for Natural Resources and Energy. FY2022 annual report on energy (Japan's energy white paper 2023). https://www.enecho.meti.go.jp/en/category/whitepaper/; 2023.

[3] Hydrogen Council. Hydrogen, Scaling up - a sustainable pathway for the global energy transition. https://hydrogencouncil.com/en/study-hydrogen-scaling-up/; 2017.

[4] International Energy Agency. Energy technology perspectives 2017. https://doi.org/10.1787/energy_tech-2017-en; 2017.

[5] International Energy Agency. The Future of Hydrogen - seizing today's opportunities. https://www.iea.org/reports/the-future-of-hydrogen; 2019.

[6] International Energy Agency. Global hydrogen review 2023. https://www.iea.org/reports/global-hydrogen-review-2023; 2023.

[7] Sasaki K, Li H-W, Hayashi A, Yamabe J, Ogura T, Lyth MS. Hydrogen energy engineering: a Japanese perspective. Japan: Springer; 2016. https://doi.org/10.1007/978-4-431-56042-5.

[8] Takahashi T, Ikeda T, Murata K, Hotaka O, Shigeki H, Tachikawa Y, Nishihara M, Matsuda J, Kitahara T, Lyth MS, Hayashi A, Sasaki K. Accelerated durability testing of fuel cell stacks for commercial automotive applications: a case study. J Electrochem Soc 2022;169:044523. https://doi.org/10.1149/1945-7111/ac662d.

[9] Takahashi T, Kokubo Y, Murata K, Hotaka O, Hasegawa S, Tachikawa Y, Nishihara M, Matsuda J, Kitahara T, Lyth MS, Hayashi A, Sasaki K. Cold start cycling durability of fuel cell stacks for commercial automotive applications. Int J Hydrogen Energy 2022;47:41111–23. https://doi.org/10.1016/j.ijhydene.2022.09.172.

[10] Toyota Motor Corporation. Toyota technical review, vol. 66; 2021. https://global.toyota/pages/global_toyota/mobility/technology/toyota-technical-review/TTR_Vol66_E.pdf.

[11] New Energy and Industrial Technology Development Organization (NEDO). NEDO fuel cell/hydrogen technology development roadmap-fuel cell roadmap for FCV/HDV. https://www.nedo.go.jp/library/battery_hydrogen.html; 2023.

[12] Cullen DA, Neyerlin KC, Ahluwalia RK, Mukundan R, More KL, Borup RL, Weber AZ, Myers DJ, Kusoglu A. New roads and challenges for fuel cells in heavy-duty transportation. Nat Energy 2021;6:462–74. https://doi.org/10.1038/s41560-021-00775-z.

[13] Larminie J, Dicks A. Fuel cell systems explained. John Wiley & Sons; 2003. https://doi.org/10.1002/9781118878330.

[14] Roen LM, Paik CH, Jarvi TD. Electrocatalytic corrosion of carbon support in PEMFC cathodes. Electrochem Solid State Lett 2004;7:A19. https://doi.org/10.1149/1.1630412.

[15] Reiser CA, Bregoli L, Patterson TW, Yi JS, Yang JD, Perry ML, Jarvi TD. A reverse-current decay mechanism for fuel cells. Electrochem Solid State Lett 2005;8:A273. https://doi.org/10.1149/1.1896466.

[16] Maass S, Finsterwalder F, Frank G, Hartmann R, Merten C. Carbon support oxidation in PEM fuel cell cathodes. J Power Sources 2008;176:444–51. https://doi.org/10.1016/j.jpowsour.2007.08.053.

[17] Taniguchi A, Akita T, Yasuda K, Miyazaki Y. Analysis of electrocatalyst degradation in PEMFC caused by cell reversal during fuel starvation. J Power Sources 2004;130:42–9. https://doi.org/10.1016/j.jpowsour.2003.12.035.

[18] Zhao X, Hayashi A, Noda Z, Kimijima K, Yagi I, Sasaki K. Evaluation of change in nanostructure through the heat treatment of carbon materials and their durability for the start/stop operation of polymer electrolyte fuel cells. Electrochim Acta 2013;97:33–41. https://doi.org/10.1016/j.electacta.2013.02.062.

[19] Park Y-C, Kakinuma K, Uchida M, Tryk DA, Kamino T, Uchida H, Watanabe M. Investigation of the corrosion of carbon supports in polymer electrolyte fuel cells using simulated start-up/shutdown cycling. Electrochim Acta 2013;91:195–207. https://doi.org/10.1016/j.electacta.2012.12.082.

[20] Xue Q, Huang J-B, Yang D-J, Li B, Zhang C-M. Enhanced PEMFC durability with graphitized carbon black cathode catalyst supports under accelerated stress testing. RSC Adv 2021;11:19417–25. https://doi.org/10.1039/D1RA01468D.

[21] Yli-Rantala E, Pasanen A, Kauranen P, Ruiz V, Borghei M, Kauppinen E, Oyarce A, Lindbergh G, Lagergren C, Darab M, Sunde S, Thomassen M, Ma-Andersen S, Skou E. Investigation of further improvement of platinum catalyst durability with highly graphitized carbon nanotubes support. Fuel Cell 2011;11:715–25. https://doi.org/10.1002/fuce.201000180.

[22] Wang J, Yin G, Shao Y, Wang Z, Gao Y. Investigation of further improvement of platinum catalyst durability with highly graphitized carbon nanotubes support. J Phys Chem C 2008;112:5784–9. https://doi.org/10.1021/JP800186P.

[23] Shao Y, Yin G, Zhang J, Gao Y. Comparative investigation of the resistance to electrochemical oxidation of carbon black and carbon nanotubes in aqueous sulfuric acid solution. Electrochim Acta 2006;51:5853–7. https://doi.org/10.1016/J.ELECTACTA.2006.03.021.

[24] Hayashi A, Notsu H, Kimijima K, Miyamoto J, Yagi I. Preparation of Pt/mesoporous carbon (MC) electrode catalyst and its reactivity toward oxygen reduction. Electrochim Acta 2008;53:6117–25. https://doi.org/10.1016/J.ELECTACTA.2008.01.110.

[25] Shanahan PV, Xu L, Liang C, Waje M, Dai S, Yan YS. Graphitic mesoporous carbon as a durable fuel cell catalyst support. J Power Sources 2008;185:423–7. https://doi.org/10.1016/J.JPOWSOUR.2008.06.041.

[26] Shao Y, Zhang S, Wang C, Nie Z, Liu J, Wang Y, Lin Y. Highly durable graphene nanoplatelets supported Pt nanocatalysts for oxygen reduction. J Power Sources 2010;195:4600–5. https://doi.org/10.1016/J.JPOWSOUR.2010.02.044.

[27] Liu J, Takeshi D, Sasaki K, Lyth SM. Platinum-decorated nitrogen-doped graphene foam electrocatalysts. Fuel Cell 2014;14:728–34. https://doi.org/10.1002/fuce.201300258.

[28] Jafri RI, Rajalakshmi N, Ramaprabhu S. Nitrogen doped graphene nanoplatelets as catalyst support for oxygen reduction reaction in proton exchange membrane fuel cell. J Mater Chem 2010;20:7114–7. https://doi.org/10.1039/c0jm00467g.

[29] Wang X, Lee JS, Zhu Q, Liu J, Wang Y, Dai S. Ammonia-treated ordered mesoporous carbons as catalytic materials for oxygen reduction reaction. Chem Mater 2010;22:2178–80. https://doi.org/10.1021/cm100139d.

[30] Marcel Pourbaix. Atlas of electrochemical equilibria in aqueous solutions. http://sunlight.caltech.edu/aic/pourbaix.pdf; 1974.

[31] Sasaki K, Takasaki F, Noda Z, Hayashi S, Shiratori Y, Ito K. Alternative electrocatalyst support materials for polymer electrolyte fuel cells. ECS Trans 2010;33(1):473–82. https://doi.org/10.1149/1.3484545.

[32] Rajalakshmi N, Lakshmi N, Dhathathreyan KS. Nano titanium oxide catalyst support for proton exchange membrane fuel cells. Int J Hydrogen Energy 2008;33:7521–6. https://doi.org/10.1016/J.IJHYDENE.2008.09.032.

[33] Akalework NG, Pan C-J, Su W-N, Rick J, Tsai M-C, Lee J-F, Lin J-M, Tsai L-D, Hwang B-J. Ultrathin TiO_2-coated MWCNTs with excellent conductivity and SMSI nature as Pt catalyst support for oxygen reduction reaction in PEMFCs. J Mater Chem 2012;22:20977. https://doi.org/10.1039/c2jm34361d.

[34] Zhang Z, Wang X, Cui Z, Liu C, Lu T, Xing W. Pd nanoparticles supported on WO_3/C hybrid material as catalyst for oxygen reduction reaction. J Power Sources 2008;185:941–5. https://doi.org/10.1016/J.JPOWSOUR.2008.07.044.

[35] Yan Z, Wei W, Xie J, Meng S, Lü X, Zhu J. An ion exchange route to produce WO_3 nanobars as Pt electrocatalyst promoter for oxygen reduction reaction. J Power Sources 2013;222:218–24. https://doi.org/10.1016/j.jpowsour.2012.08.070.

[36] Yan Z, Xie J, Jing J, Zhang M, Wei W, Yin S. MoO_2 nanocrystals down to 5 nm as Pt electrocatalyst promoter for stable oxygen reduction reaction. Int J Hydrogen Energy 2012;37:15948–55. https://doi.org/10.1016/J.IJHYDENE.2012.08.033.

[37] Ohnishi R, Takahashi Y, Takagaki A, Kubota J, Domen K. Niobium oxides as cathode electrocatalysts for platinum-free polymer electrolyte fuel cells. Chem Lett 2008;37:838–9. https://doi.org/10.1246/cl.2008.838.

[38] Kuroki T, Sasaki K, Kusaba H, Teraoka Y. PEFC electrode catalysts supported on nanocrystalline semiconducting oxides. Extended Abstract #1527, 206th Meeting of Electrochem Soc, Hawaii 2004. https://www.electrochem.org/dl/ma/206/pdfs/1527.pdf.

[39] Masao A, Noda S, Takasaki F, Ito K, Sasaki K. Carbon-free Pt electrocatalysts supported on SnO_2 for polymer electrolyte fuel cells. Electrochem Solid State Lett 2009;12:B119. https://doi.org/10.1149/1.3152325.

[40] Takasaki F, Matsuie S, Takabatake Y, Noda Z, Hayashi A, Shiratori Y, Ito K, Sasaki K. Carbon-free Pt electrocatalysts supported on SnO_2 for polymer electrolyte fuel cells: electrocatalytic activity and durability. J Electrochem Soc 2011;158:B1270. https://doi.org/10.1149/1.3625918.

[41] Tsukatsune T, Takabatake Y, Noda Z, Daio T, Zaitsu A, Lyth SM, Hayashi A, Sasaki K. Platinum-decorated tin oxide and niobium-doped tin oxide PEFC electrocatalysts: oxygen reduction reaction activity. J Electrochem Soc 2014;161:F1208–13. https://doi.org/10.1149/2.0431412jes.

[42] Nakazato Y, Kawachino D, Noda Z, Matsuda J, Lyth SM, Hayashi A, Sasaki K. PEFC electrocatalysts supported on Nb-SnO_2 for MEAs with high activity and durability: Part I. Application of different carbon fillers. J Electrochem Soc 2018;165:F1154–63. https://doi.org/10.1149/2.0311814jes.

[43] Matsumoto S, Nagamine M, Noda Z, Matsuda J, Lyth SM, Hayashi A, Sasaki K. PEFC electrocatalysts supported on Nb-SnO_2 for MEAs with high activity and durability: Part II. Application of bimetallic Pt-alloy catalysts. J Electrochem Soc 2018;165:F1164–75. https://doi.org/10.1149/2.0321814jes.

[44] Inoue Y, Yasutake M, Noda Z, Lyth SM, Nishihara M, Hayashi A, Matsuda J, Sasaki K. Preparation of nanocrystalline Nb-doped SnO_2 on mesoporous carbon for PEFC electrocatalysts. ECS Trans 2022;109(9):413–23. https://doi.org/10.1149/10909.0413ecst.

[45] Kakinuma K, Uchida M, Kamino T, Uchida H, Watanabe M. Synthesis and electrochemical characterization of Pt catalyst supported on $Sn_{0.96}Sb_{0.04}O_{2-\delta}$ with a network structure. Electrochim Acta 2011;56:2881–7. https://doi.org/10.1016/j.electacta.2010.12.077.

[46] Kakinuma K, Chino Y, Senoo Y, Uchida M, Kamino T, Uchida H, Deki S, Watanabe M. Characterization of Pt catalysts on Nb-doped and Sb-doped $SnO_{2-\delta}$ support materials with aggregated structure by rotating disk electrode and fuel cell measurements. Electrochim Acta 2013;110:316–24. https://doi.org/10.1016/J.ELECTACTA.2013.06.127.

[47] Shao-Horn Y, Sheng WC, Chen S, Ferreira PJ, Holby EF, Morgan D. Instability of supported platinum nanoparticles in low-temperature fuel cells. Top Catal 2007;46:285–305. https://doi.org/10.1007/s11244-007-9000-0.

[48] Ferreira PJ, la O'GJ, Shao-Horn Y, Morgan D, Makharia R, Kocha S, Gasteiger HA. Instability of Pt/C electrocatalysts in proton exchange membrane fuel cells. J Electrochem Soc 2005;152:A2256. https://doi.org/10.1149/1.2050347.

[49] Takenaka S, Goto M, Masuda Y, Emura S, Kishida M. Improvement in the durability of carbon black-supported Pt cathode catalysts by silica-coating for use in PEFCs. Int J Hydrogen Energy 2018;43:7473–82. https://doi.org/10.1016/J.IJHYDENE.2018.02.159.

[50] Schmies H, Hornberger E, Anke B, Jurzinsky T, Nong HN, Dionigi F, Kühl S, Drnec J, Lerch M, Cremers C, Strasser P. Impact of carbon support functionalization on the electrochemical stability of Pt fuel cell catalysts. Chem Mater 2018;30:7287–95. https://doi.org/10.1021/acs.chemmater.8b03612.

[51] Zhao X, Takao S, Higashi K, Kaneko T, Samjeskè G, Sekizawa O, Sakata T, Yoshida Y, Uruga T, Iwasawa Y. Simultaneous improvements in performance and durability of an octahedral $PtNi_x$/C electrocatalyst for next-generation fuel cells by

continuous, compressive, and concave Pt skin layers. ACS Catal 2017;7:4642–54. https://doi.org/10.1021/acscatal.7b00964.

[52] Hayashi A, Kimijima K, Miyamoto J, Yagi I. Oxygen transfer and storage processes inside the mesopores of platinum-deposited mesoporous carbon catalyst thin-layer electrode. J Phys Chem C 2009;113:12149–53. https://doi.org/10.1021/jp901298r.

[53] Song S, Liang Y, Li Z, Wang Y, Fu R, Wu D, Tsiakaras P. Effect of pore morphology of mesoporous carbons on the electrocatalytic activity of Pt nanoparticles for fuel cell reactions. Appl Catal, B 2010;98:132–7. https://doi.org/10.1016/J.APCATB.2010.05.021.

[54] Minamida Y, Noda Z, Hayashi A, Sasaki K. Development of MEAs with Pt/mesoporous carbon as a cathode catalyst. ECS Trans 2014;64(3):137–44. https://doi.org/10.1149/06403.0137ecst.

[55] Padgett E, Yarlagadda V, Holtz ME, Ko M, Levin BDA, Kukreja RS, Ziegelbauer JM, Andrews RN, Ilavsky J, Kongkanand A, Muller DA. Mitigation of PEM fuel cell catalyst degradation with porous carbon supports. J Electrochem Soc 2019;166:F198–207. https://doi.org/10.1149/2.0371904jes.

[56] Daio T, Staykov A, Guo L, Liu J, Tanaka M, Lyth SM, Sasaki K. Lattice strain mapping of platinum nanoparticles on carbon and SnO_2 supports. Sci Rep 2015;5:13126. https://doi.org/10.1038/srep13126.

[57] Rumble JR, editor. Handbook of chemistry and physics. 104th Edition. CRC Press. Taylor & Francis Group; 2023. ISBN 9781032425207.

[58] Awaludin Z, Moo JGS, Okajima T, Ohsaka T. TaO_x-capped Pt nanoparticles as active and durable electrocatalysts for oxygen reduction. J Mater Chem A 2013;1:14754–65. https://doi.org/10.1039/c3ta12492d.

[59] Gao W, Zhang Z, Dou M, Wang F. Highly dispersed and crystalline Ta_2O_5 anchored Pt electrocatalyst with improved activity and durability toward oxygen reduction: promotion by atomic-scale Pt−Ta_2O_5 interactions. ACS Catal 2019;9:3278–88. https://doi.org/10.1021/acscatal.8b04505.

[60] Miyamoto R, Ogawa T, Nishiizumi R, Yasutake M, Noda Z, Nishihara M, Hayashi A, Matsuda J, Sasaki K. Pt-Ta-Co electrocatalysts for polymer electrolyte fuel cells. ECS Trans 2023;112(4):353–60. https://doi.org/10.1149/11204.0353ecst.

[61] Inaba M, Ito H, Tsuji H, Wada T, Banno M, Yamada H, Saito M, Tasaka A. Effect of core size on activity and durability of Pt core-shell catalysts for PEFCs. ECS Trans 2010;33(1):231–8. https://doi.org/10.1149/1.3484520.

[62] Mani P, Srivastava R, Strasser P. Dealloyed binary PtM_3 (M = Cu, Co, Ni) and ternary $PtNi_3M$ (M = Cu, Co, Fe, Cr) electrocatalysts for the oxygen reduction reaction: performance in polymer electrolyte membrane fuel cells. J Power Sources 2011;196:666–73. https://doi.org/10.1016/J.JPOWSOUR.2010.07.047.

[63] New Energy and Industrial Technology Development Organization (NEDO). NEDO PEFC cell evaluation and analysis protocol. https://www.nedo.go.jp/content/100963953.pdf; 2023.

[64] Ogawa T, Inoue Y, Yamamoto K, Yasutake M, Noda Z, Lyth SM, Matsuda J, Nishihara M, Hayashi A, Sasaki K. Power generation performance of polymer electrolyte fuel cells with electrocatalysts supported on SnO_2 in high current density range. ECS Trans 2022;109(9):241–9. https://doi.org/10.1149/10909.0241ecst.

[65] Katayama S, Matsumoto M, Imai H, Asaoka T, Amemiya K. Comparison of MEA degradation through FCV actual driving test and load-cycle durability test. ECS Trans 2023;112(4):157–65. https://doi.org/10.1149/11204.0157ecst.

[66] Ogawa T, Nakamura S, Miyamoto R, Yasutake M, Noda Z, Matsuda J, Nishihara M, Hayashi A, Sasaki K. Power generation characteristics of polymer electrolyte fuel cells with electrocatalysts supported on SnO_2 in high current density range. ECS Trans 2023;112(4):215–23. https://doi.org/10.1149/11204.0215ecst.